European Journal of Mechanics / B Fluids 112 (2025) 1–9

Contents lists available at ScienceDirect

European Journal of Mechanics / B Fluids

journal homepage: www.elsevier.com/locate/ejmflu

Unsteady Couette flow of a class of fluids described by non-monotone models

Lorenzo Fusi, Antonio Giovinetto, Rebecca Tozzi *

Università degli Studi di Firenze, Dipartimento di Matematica e Informatica "Ulisse Dini", Viale Morgagni 67/A, 50134 Firenze, Italy

ARTICLE INFO

Keywords:
Couette flow
Non-monotone model
Spectral collocation method

ABSTRACT

In this paper we study the unsteady Couette motion of an incompressible non-linear fluid driven by a prescribed shear stress or a prescribed velocity imposed on the top surface. The fluid under consideration is described by a non-monotone relation between stress and strain rate. We consider the two-dimensional unsteady problem and solve it numerically by means of Crank–Nicolson scheme combined with spectral collocation method. We investigate the time behaviour of the velocity field, in order to find out, starting from suitable initial conditions, whether the numerical solutions tend to the corresponding stationary one or not. Our results confirm both the stability of the two solutions belonging to the ascending branches of the constitutive law and the linear instability of the one on the descending branch.

1. Introduction

Modelling of the behaviour of Newtonian or non-Newtonian fluids can be achieved by the specification of the constitutive relation which describes the response of the fluid to a given stimuli. In the case of complex fluids, this relation may be highly involved and, moreover, it could not be possible to express a specific kinematical quantity as a function of the other variables (see e.g. [1–8]). In [1], for instance, Rajagopal introduced an implicit algebraic constitutive relation between the Cauchy stress tensor and the strain rate tensor, providing a significant change of perspective in modelling fluid-like materials [9]. Further generalizations have been provided by many researchers (see e.g. [9–15]). In particular, in [14] Malek et al. studied a class of fluids in whose model the symmetric part of the velocity gradient is expressed as a power-function of the deviatoric part of the Cauchy stress tensor. Le Roux and Rajagopal [15] modified this model, and the modification allows one to fit experimental data for flows of colloids very well [10]. They investigated simple shear flows of the constitutive relation they had proposed, between two parallel plates. Fusi et al. [10] have studied the flow of a fluid described by this non-monotone law in an orthogonal rheometer looking for pseudo-planar solutions. They found that pronounced boundary layers adjacent to the rotating plates may develop even at low Reynolds number. Many complex fluids, such as blood, colloidal suspensions, polymer solutions, etc., can be modelled by using this non-monotone law as constitutive law. In particular, we refer the reader to the papers [14,15] and the references therein for examples of real fluids that show a constitutive behaviour like the one considered in this paper. Among these, we mention coagulated blood, in which viscosity is far greater than the viscosity of normal blood and causes a reduction in the shear rate of the blood, see [16–19].

Recently, Calusi et al. [9] have investigated the onset of instability of a Couette flow driven by a shear stress, assuming that the fluid obeys to a non-monotone relation between stress and strain rate. They provided a range for the Reynolds number for which three basic steady flows are possible and they performed a linear stability analysis for each of them. They proved that the two basic solutions belonging to the ascending branches of the constitutive law are unconditionally stable, while the one corresponding to the descending branch is unconditionally unstable.

The aim of this paper is to study the unsteady 2D Couette flow driven by a prescribed shear stress imposed on the top surface (i.e. Neumann boundary conditions), considering the class of fluids characterized by the non-monotone curve studied in [9]. In this model, for certain values of the material parameters, the stress can be expressed as a function of the strain-rate but not vice-versa. This is due to the non-monotonicity of the stress vs strain rate relation, that prevents us from expressing the strain rate tensor $\mathbb{D}^*$[1] as a function of the deviatoric stress tensor $\mathbb{S}^*$. We investigate the same problem with different boundary conditions too, i.e. Dirichlet boundary conditions, imposing a prescribed velocity on the top surface. Moreover, we include in our analysis also the case of monotone relation between stress and strain rate thanks to the choice of different values of the involved parameters. The problem is always solved numerically via spectral collocation method based on Chebyshev polynomials.

* Corresponding author.
E-mail address: rebecca.tozzi@unifi.it (R. Tozzi).

[1] Starred variables denote dimensional quantities.

https://doi.org/10.1016/j.euromechflu.2025.02.005
Received 8 October 2024; Received in revised form 23 January 2025; Accepted 14 February 2025
Available online 22 February 2025
0997-7546/© 2025 The Authors. Published by Elsevier Masson SAS. This is an open access article under the CC BY-NC-ND license (http://creativecommons.org/licenses/by-nc-nd/4.0/).

In particular, using the non-monotone model, we are interested in making a comparison between our numerical results and the stability results obtained in [9], in order to find whether they match or not. More precisely, we want to see if, starting from a configuration sufficiently close to the steady state solution belonging to one of the ascending branches of the constitutive law, the numerical solution tends to the corresponding stable solution in the two different cases of boundary conditions. On the other hand, we expect that, neither assuming Neumann nor Dirichlet boundary conditions, this happens in the case of the unstable steady state solution on the descending branch. If instead we assume the monotone relation, we suspect that the unique steady state solution of the problem is stable and can be reached starting from an initial condition in an "appropriate" neighbourhood of the stationary one. We remark that the numerical method we have adopted is not "important" and that we could have used other methods, such as finite differences or finite elements to get the numerical solution. The focus of this paper is indeed the confirmation of the results of the linear stability analysis performed in [9].

The paper is organized as follows: in Section 2 we present the mathematical problem under the hypothesis of the two different types of boundary conditions. In both cases, it consists in an unsteady boundary value problem whose unknowns are the components of the deviatoric part of the stress, of the velocity field and pressure. In Section 3 we look for a one-dimensional steady solution for the two problems and we recover the three basic flows determined in [9]. We also perform the same analysis in the case of monotone relation between stress and strain rate. Then, in Section 4 we introduce the numerical scheme we have used to solve the problems based on the Crank–Nicolson algorithm combined with spectral collocation method. Finally, in Section 5 we discuss the results obtained and, in particular, we show the agreement between our numerical findings and the stability results of Calusi et al. [9].

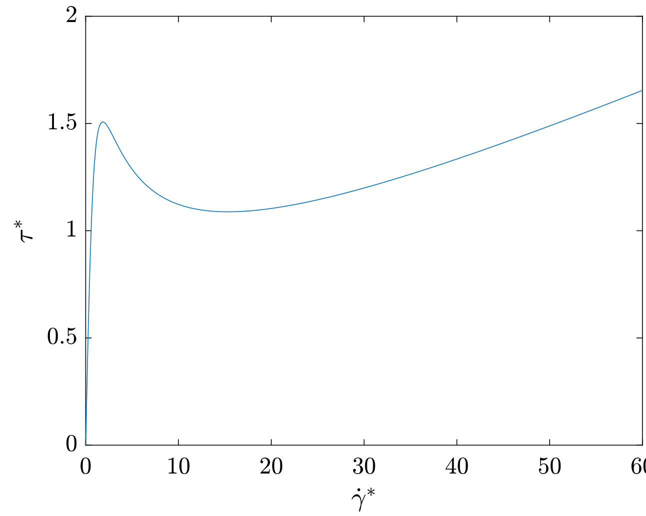

Fig. 1. Plot of the shear stress τ^* in function of the strain rate $\dot\gamma^*$ with the characteristic "S-shape".

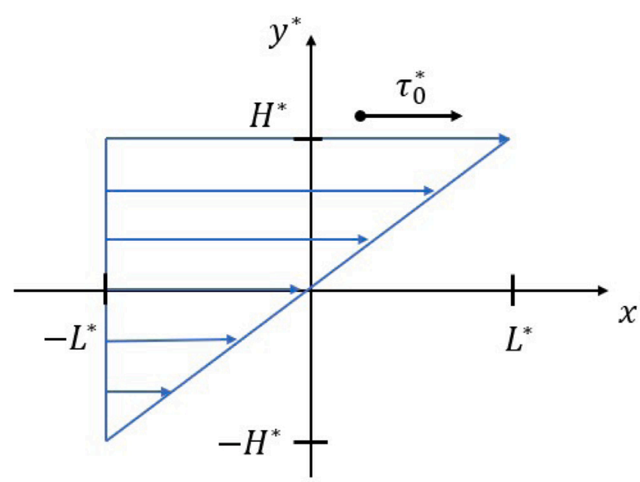

Fig. 2. Geometry of the problem.

2. The mathematical model

2.1. Neumann boundary conditions

We investigate the Couette flow between parallel plates driven by a prescribed shear stress imposed on the top surface of a fluid layer. We consider a class of incompressible non-Newtonian fluids obeying the non-monotone model (see [15]) and characterized by the following constitutive relation

$$\mathbb{T}^* = -p^*\mathbb{I} + \mathbb{S}^*, \tag{1}$$

where

$$\mathbb{S}^* = 2\mu^*(\dot\gamma^*)\mathbb{D}^*, \qquad \mu^*(\dot\gamma^*) = \mu_0^*\left[\left(1+\alpha^*\dot\gamma^{*2}\right)^n + \beta\right], \qquad \dot\gamma^* = \sqrt{\frac{1}{2}\,\mathbb{D}^*\cdot\mathbb{D}^*}. \tag{2}$$

In (1), (2) $-p^*\mathbb{I}$ is the indeterminate part of the stress due to the constraint of incompressibility, $\mathbb{S}^*$ is the deviatoric part of the stress, $\dot\gamma^*$ is the Frobenius norm of the symmetric part of the velocity gradient $\mathbb{D}^*$, μ_0^* is a reference viscosity, α^* is a positive real quantity whose dimension is that of a squared time, n and β are non-dimensional real parameters ($\beta > 0$).

In [15] it is proved that, if

$$n < -\frac{1}{2} \qquad \text{and} \qquad \beta < 2\left[\frac{|2n+1|}{2(1-n)}\right]^{1-n}, \tag{3}$$

the norm $\tau^* = \sqrt{\frac{1}{2}\,\mathbb{S}^*\cdot\mathbb{S}^*}$ is a non monotone function of $\dot\gamma^*$. In this case the function τ^* vs $\dot\gamma^*$ exhibits the curve shown in Fig. 1.

The flow is assumed to be 2D with a velocity field of the form (see Fig. 2)

$$\mathbf{v}^* = u^*(x^*, y^*, t^*)\ \mathbf{e}_x + v^*(x^*, y^*, t^*)\ \mathbf{e}_y.$$

The equations governing the unsteady flow of our incompressible fluid can be written as (we are neglecting volume forces)

$$\begin{cases} \rho^*\left(\mathbf{v}^*_{t^*} + (\nabla\mathbf{v}^*)\mathbf{v}^*\right) = -\nabla p^* + \operatorname{div}(\mathbb{S}^*), \\ \operatorname{div}(\mathbf{v}^*) = 0. \end{cases} \tag{4}$$

We consider a Couette flow driven by a shear stress τ_0^* imposed on the top surface, assuming that no pressure gradient contributes to the flow (see Fig. 2). The thickness of the layer is assumed to be fixed and equal to $2H^*$ and we focus on a portion of length $2L^*$. Since no horizontal pressure drop is acting, we may safely assume that on the boundary $x^* = \pm L^*$ pressure is constant, i.e. $p^* = p_0^*$. The boundary conditions for the velocity field are no-slip at the lower wall of the channel and zero transversal velocity at the inlet and outlet $x^* = \pm L^*$:

$$u^*(x^*, y^* = -H^*, t^*) = 0, \quad v^*(x^*, y^* = -H^*, t^*) = 0,$$
$$v^*(x^* = \pm L^*, y^*, t^*) = 0.$$

The boundary conditions for the stress come from the assumption of a pure shear stress imposed on the upper wall of the channel (i.e. Neumann boundary conditions), namely:

$$S_{12}^*(x^*, y^* = H^*, t^*) = \tau_0^*, \quad S_{22}^*(x^*, y^* = H^*, t^*) = 0.$$

The boundary conditions for the pressure are given imposing the constant inlet and outlet pressure:

$$p^*(x^* = \pm L^*, y^*, t^*) = p_0^*.$$

We introduce the aspect ratio

$$\delta = \frac{H^*}{L^*},$$

and we rescale the variables as

$$x^* = L^* x, \qquad y^* = H^* y, \qquad t^* = \left(\frac{L^*}{U^*}\right)t, \qquad u^* = U^* u,$$
$$v^* = \left(\delta U^*\right)v, \qquad p^* = P^* p + p_0^*, \qquad \mathbb{D}^* = \left(\frac{U^*}{H^*}\right)\mathbb{D}, \qquad \dot\gamma^* = \left(\frac{U^*}{H^*}\right)\dot\gamma,$$
$$\mathbb{S}^* = \left(\mu_0^* \frac{U^*}{H^*}\right)\mathbb{S}, \qquad \alpha^* = \left(\frac{H^{*2}}{U^{*2}}\right)\alpha, \qquad \mu^* = \mu_0^* \mu(\dot\gamma),$$

where U^* and P^* are characteristic velocity and pressure yet to be specified.

We get

$$\mathbb{D} = \frac{1}{2}\begin{pmatrix} 2\delta u_x & u_y + \delta^2 v_x \\ u_y + \delta^2 v_x & 2\delta v_y \end{pmatrix} \quad \text{and} \quad \mathbb{S} = 2\mu(\dot\gamma)\mathbb{D} = \begin{pmatrix} S_{11} & S_{12} \\ S_{12} & S_{22} \end{pmatrix}.$$

The non-dimensional versions of (2) are

$$\dot\gamma = \sqrt{\delta^2 (u_x)^2 + \frac{1}{4}(u_y + \delta^2 v_x)^2}, \quad \mu(\dot\gamma) = (1 + \alpha\dot\gamma^2)^n + \beta,$$
$$\tau = 2\mu(\dot\gamma)\dot\gamma = 2\left[(1 + \alpha\dot\gamma^2)^n + \beta\right]\dot\gamma. \tag{5}$$

Selecting $P^* = (\mu_0^*\, U^* L^*)/H^{*2}$ and defining the Reynolds number as

$$Re = \left(\frac{\rho^* U^* H^*}{\mu_0^*}\right),$$

we can write the complete system in the stress-based formulation

$$\begin{cases} Re\ \delta(u_t + u_x u + u_y v) = -p_x + \delta(S_{11})_x + (S_{12})_y, \\ Re\ \delta^3(v_t + v_x u + v_y v) = -p_y + \delta^2(S_{12})_x + \delta(S_{22})_y, \\ u_x + v_y = 0, \\ S_{11} = 2\delta\mu(\dot\gamma)\ u_x, \\ S_{12} = \mu(\dot\gamma)(u_y + \delta^2 v_x), \\ S_{22} = 2\delta\mu(\dot\gamma)\ v_y, \end{cases} \tag{6}$$

with the following boundary conditions

$$\begin{cases} (S_{12})\big|_{y=1} = \tau_0, \\ u\big|_{y=-1} = 0, \\ (S_{22})\big|_{y=1} = 0, \\ v\big|_{x=\pm 1} = 0, \\ v\big|_{y=-1} = 0, \\ p\big|_{x=\pm 1} = p_0, \end{cases} \tag{7}$$

where τ_0 and p_0 are the non-dimensional versions of τ_0^* and p_0^* respectively, that is

$$\tau_0 := \left(\frac{H^*}{\mu_0^* U^*}\right)\tau_0^*, \quad p_0 := 0.$$

The problem (6),(7) for the unknowns S_{11}, S_{12}, S_{22}, u, v, p will be solved numerically in Section 5 combined with appropriate initial conditions.

2.2. Dirichlet boundary conditions

Now we still consider the Couette flow between parallel plates but this time driven by a prescribed longitudinal velocity imposed on the top surface. The model under consideration is the same of Section 2.1, meaning that we take again parameters that fulfil (3) and consequently the relation between stress and strain rate is still represented by the curve displayed in Fig. 1.

The difference with respect to the previous subsection consists on the boundary conditions on the upper wall, where we assume that the flow is generated by a longitudinal velocity u_0^*, namely:

$$u^*(x^*, y^* = H^*, t^*) = u_0^*, \quad v^*(x^*, y^* = H^*, t^*) = 0.$$

The governing equations are the same as before, and so we end up with the non-dimensional system (6) with the following boundary conditions

$$\begin{cases} u\big|_{y=1} = u_0, \\ u\big|_{y=-1} = 0, \\ v\big|_{y=\pm 1} = 0, \\ v\big|_{x=\pm 1} = 0, \\ p\big|_{x=\pm 1} = p_0, \end{cases} \tag{8}$$

where u_0 is the non-dimensional version of u_0^*, that is

$$u_0 := \left(\frac{1}{U^*}\right)u_0^*.$$

The problem (6),(8) for the unknowns S_{11}, S_{12}, S_{22}, u, v, p will be solved numerically in Section 5 combined with appropriate initial conditions.

3. 1D solutions

We start looking for a one dimensional steady solution, namely

$$\mathbf{v} = u(y)\ \mathbf{e}_x,$$

so that system (6) reduces to

$$\begin{cases} -p_x + (S_{12})_y = 0, \\ -p_y = 0, \\ S_{12} = \mu(\dot\gamma) u_y, \end{cases} \tag{9}$$

with

$$S_{11} = S_{22} = 0, \quad \dot\gamma = \frac{|u_y|}{2}. \tag{10}$$

Inserting (10) in (5), we get the shear stress τ in terms of u_y:

$$\tau(u_y) = \left[\left(1 + \alpha\frac{u_y^2}{4}\right)^n + \beta\right]|u_y|.$$

Then, since there is no pressure gradient, from (9) we find that S_{12} must be constant.

3.1. Neumann boundary conditions

Under the hypothesis of a prescribed shear stress, we obtain that

$$S_{12} \equiv \text{constant} = \tau_0 \tag{11}$$

and moreover, using (10) and (11) in the third equation of (9), we get the following algebraic equation

$$\left[\left(1 + \alpha\frac{u_y^2}{4}\right)^n + \beta\right] u_y = \tau_0. \tag{12}$$

We can look at (12) as a function of u_y, namely

$$f(u_y) = \left[\left(1 + \alpha\frac{u_y^2}{4}\right)^n + \beta\right] u_y = \tau_0, \tag{13}$$

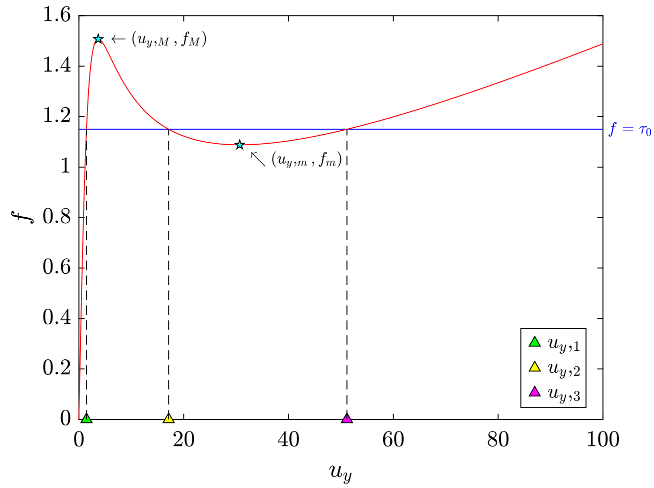

Fig. 3. Plot of f in function of u_y for $n = -0.7$, $\beta = 0.01$, $\alpha = 0.8$, $\mathrm{Re} = 1$ with $f_m = 1.0883 < \tau_0 = 1.15 < f_M = 1.5071$. The three distinct solutions are $u_{y,1} = 1.45414$, $u_{y,2} = 17.1281$, $u_{y,3} = 51.1502$.

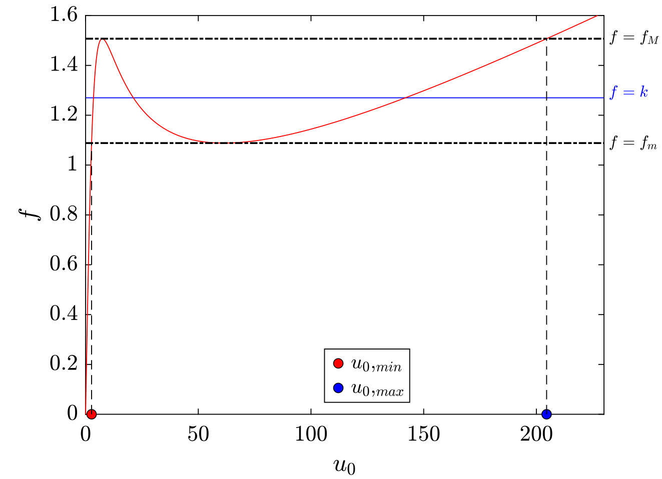

Fig. 4. Plot of f in function of u_0 for $n = -0.7$, $\beta = 0.01$, $\alpha = 0.8$, $\mathrm{Re} = 1$ with $f(u_0 = 3.5) = k = 1.27$. Condition (17) is equivalent to $2.6566 < u_0 < 204.5378$. The three distinct solutions are $u_{y,1} = 1.74991$, $u_{y,2} = 10.5968$, $u_{y,3} = 70.9461$.

where α, n and β are parameters which depend only on the geometry of the problem and on the material under consideration. Moreover, once we have fixed n and β fulfilling (3), f is a non-monotone function of u_y (see [15]) exhibiting a local maximum and minimum, that we denote by $u_{y,M}$ and $u_{y,m}$ respectively (see Fig. 3). Setting $f_M = f(u_{y,M})$ and $f_m = f(u_{y,m})$, we find that Eq. (12) is satisfied by three distinct values of u_y, which we denote by $u_{y,1}$, $u_{y,2}$, $u_{y,3}$, under the hypothesis that

$$f_m < \tau_0 < f_M. \tag{14}$$

In particular, when (14) is fulfilled, we order the three solutions in increasing order, i.e. $u_{y,1} < u_{y,2} < u_{y,3}$, so that the first and the third ones belong to the ascending branches of f, while the second one is on the descending branch. These are the same stationary solutions determined in [9], where it is proved that $u_{y,1}$ and $u_{y,3}$ are (linearly) unconditionally stable, while $u_{y,2}$ is (linearly) unconditionally unstable.

Remark. If we replace the constitutive Eq. (5) by that studied in Le Roux and Rajagopal in [15], where the shear rate is a non-monotonic function of the shear stress (e.g. $\dot{\gamma} = g(\tau)$), the shear stress becomes a multi-valued function of the shear rate. In this case, a fixed shear rate corresponds to multiple shear stresses. Specifically, we would have three distinct base shear stresses associated with the same shear rate. These three states correspond to two ascending branches and one descending branch of the flow curve. We expect that the base state associated with the descending branch is unstable, while the other two are stable, but we are not able to make a comparison using this method because this should be confirmed through a rigorous linear stability analysis.

3.2. Dirichlet boundary conditions

In the case of a prescribed longitudinal velocity, as we have done in the previous subsection and using the same notations, we obtain that

$$f(u_y) = k, \tag{15}$$

where k is a constant value. From (15) we deduce that u has to be a linear function of y, namely $u(y) = Ay + B$, where A and B are constant to be determined by imposing the first two boundary conditions of (8). Therefore, we get the following expression for the velocity

$$u(y) = \frac{u_0}{2}\left(y + 1\right). \tag{16}$$

Now, using (16) in (15) and selecting again n and β fulfilling (3), we can do the same considerations as in Section 3.1, and we can recover a condition that the velocity on the upper plate has to satisfy in order to have the existence of the three different solutions of Eq. (15). In other words, looking at f as a function of u_0, we have to select u_0 fulfilling

$$f_m < k < f_M \iff f_m < \left[\left(1 + \alpha\frac{u_0^2}{16}\right)^n + \beta\right]\frac{u_0}{2} < f_M, \tag{17}$$

as shown in Fig. 4. We expect that the linear stability analysis of the three stationary solutions remains unchanged with respect to the previous case.

3.3. Monotone case with Neumann boundary conditions

Now we assume to have a monotone relation between stress and strain rate (see Fig. 5), that is to take values of n and β which do not satisfy (3). We are considering to have a prescribed shear stress imposed on the top surface, as in the non-monotone case with Neumann boundary conditions. As we have done in Section 3.1, we get Eq. (13). The difference consists on the fact that now it admits a single solution, which we denote by $u_{y,1}$, for every value of the prescribed shear stress τ_0, as shown in Fig. 5. We expect that this state solution is linear unconditionally stable, as shown in [9].

4. Numerical scheme

We assume that n, β, τ_0 and u_0 fulfil conditions (3), (14), (17) respectively, so that in both cases there exist three distinct solutions, as observed in Section 3. We solve numerically via MATLAB the two unsteady boundary value problems (6), (6) and (7), (8) obtained in Section 2 enforced with appropriate initial conditions. To this aim, we perform a time-discretization of the problems using Crank–Nicolson method (see [20]), i.e. a finite difference method based on the fact that a generic partial differential equation of the form

$$\partial_t h = H\left(h, x, y, t, \partial_x h, \partial_y h\right)$$

can be discretized as

$$h^{k+1} - h^k = \frac{\Delta t}{2}\left[H^{k+1} + H^k\right],$$

where $h^k := h(x, y, k\Delta t)$, $H^k := H(h^k, x, y, k\Delta t, \partial_x h^k, \partial_y h^k)$ and the superscript k indicates the iteration k. During each loop of Crank–Nicolson algorithm, we use a spectral collocation method based on Chebyshev polynomials to discretize the system in space.

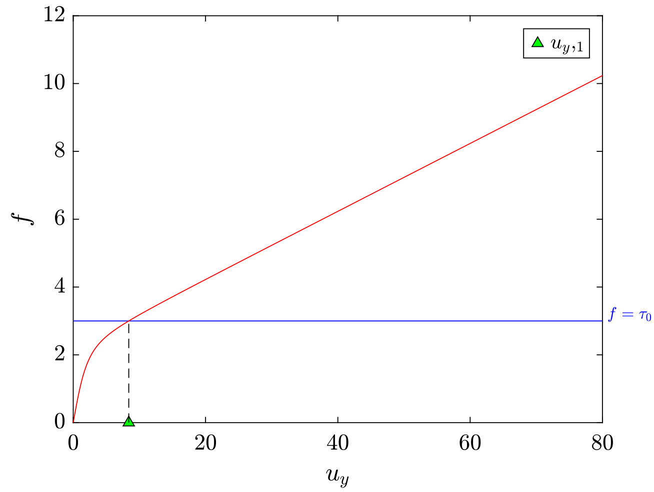

Fig. 5. Plot of f in function of u_y for $n = -0.5$, $\beta = 0.1$, $\alpha = 0.8$, Re $= 1$ with $\tau_0 = 3$. The single solution is $u_{y,1} = 8.39301$.

The flow domain is the square centred at the origin of the Cartesian system with side length two, i.e. $[-1, 1]^2$. We use a grid of $(N+1)\times(N+1)$ ($N = 15$) Gauss–Lobatto points clustered at the boundaries of $[-1, 1]^2$. These points are put in a "lexicographic" order (see Fusi et al. [21,22] and Trefethen [23] for details), so that the $(N + 1) \times (N + 1)$ array of nodes is transformed in a $(N + 1)^2$ vector. As in [21], we denote by b_{in} the indices[2] of the inlet nodes except corners, by b_{out} the indices of the outlet nodes except corners, by b_{up} the indices of the upper edge nodes and by b_{down} the indices of the lower edge nodes. The spectral partial derivatives in the (x, y) coordinates are given by

$$\partial_x \approx D_x = D \otimes_K I, \quad \partial_y \approx D_y = I \otimes_K D, \tag{18}$$

where D is the $(N+1)\times(N+1)$ differentiation matrix defined in [23], I is the $(N+1)\times(N+1)$ identity matrix and $\otimes_K$ is the Kronecker product[3]. In particular, the dimensions of D_x and D_y are $(N + 1)^2 \times (N + 1)^2$ and these matrices operate on grid nodes put in the lexicographic order. Using the approximations (18), the whole problem (6) can be rewritten as follows

$$\begin{cases} \text{Re }\delta u_N^{k+1} + \dfrac{\Delta t}{2}\Big[\text{Re }\delta\Big((P_1 u_N^{k+1})u_N^{k+1} + (P_2 u_N^{k+1})v_N^{k+1}\Big) + P_1 p_N^{k+1} \\ \quad -\delta P_1 S_{11,N}^{k+1} - P_2 S_{12,N}^{k+1}\Big] \\ \quad -\text{Re }\delta u_N^{k} + \dfrac{\Delta t}{2}\Big[\text{Re }\delta\Big((P_1 u_N^{k})u_N^{k} + (P_2 u_N^{k})v_N^{k}\Big) + P_1 p_N^{k} - \delta P_1 S_{11,N}^{k} \\ \quad -P_2 S_{12,N}^{k}\Big] = 0, \\ \text{Re }\delta^3 v_N^{k+1} + \dfrac{\Delta t}{2}\Big[\text{Re }\delta^3\Big((P_1 v_N^{k+1})u_N^{k+1} + (P_2 v_N^{k+1})v_N^{k+1}\Big) + P_2 p_N^{k+1} \\ \quad -\delta^2 P_1 S_{12,N}^{k+1} - \delta P_2 S_{22,N}^{k+1}\Big] \\ \quad -\text{Re }\delta^3 v_N^{k} + \dfrac{\Delta t}{2}\Big[\text{Re }\delta^3\Big((P_1 v_N^{k})u_N^{k} + (P_2 v_N^{k})v_N^{k}\Big) + P_2 p_N^{k} \\ \quad -\delta^2 P_1 S_{12,N}^{k} - \delta P_2 S_{22,N}^{k}\Big] = 0, \\ P_1 u_N^{k+1} + P_2 v_N^{k+1} = 0, \\ S_{11,N}^{k+1} - 2\delta\mu_N^{k+1} P_1 u_N^{k+1} = 0, \\ S_{12,N}^{k+1} - \mu_N^{k+1}(P_2 u_N^{k+1} + \delta^2 P_1 v_N^{k+1}) = 0, \\ S_{22,N}^{k+1} - 2\delta\mu_N^{k+1} P_2 v_N^{k+1} = 0, \end{cases} \tag{19}$$

where, using (5),

$$\mu_N^{k+1} = \mu_N^{k+1}(\dot\gamma_N^{k+1}), \quad \dot\gamma_N^{k+1} = \sqrt{\delta^2\big(P_1 u_N^{k+1}\big)^2 + \frac{1}{4}\big(P_2 u_N^{k+1} + \delta^2 P_1 v_N^{k+1}\big)^2}. \tag{20}$$

In (19), (20), P_1 and P_2 are the discretized form of ∂_x and ∂_y respectively, the subscript N indicates the discretized form of the involved variables, the apex k indicates the data at time step k. At the end of every loop, the initial conditions are updated with the variables determined during the time iteration that has just ended. Moreover, each of the six unknowns $S_{11,N}$, $S_{12,N}$, $S_{22,N}$, u_N, v_N, p_N is in the form of a vector of $(N + 1)^2$ elements, according to the lexicographic order, and system (19) has dimensions $6(N + 1)^2 \times 6(N + 1)^2$.

Then, we discretize the boundary conditions (7) and (8) as follows

$$\begin{cases} B_{up}\ S_{12,N}^{k+1} = \tau_0, \\ B_{down}\ u_N^{k+1} = 0, \\ B_{up}\ S_{22,N}^{k+1} = 0, \\ B_{lat}\ v_N^{k+1} = 0, \\ B_{down}\ v_N^{k+1} = 0, \\ B_{lat}\ p_N^{k+1} = p_0, \end{cases} \tag{21}$$

and

$$\begin{cases} B_{up}\ u_N^{k+1} = u_0, \\ B_{down}\ u_N^{k+1} = 0, \\ B_{up}\ v_N^{k+1} = 0, \\ B_{lat}\ v_N^{k+1} = 0, \\ B_{down}\ v_N^{k+1} = 0, \\ B_{lat}\ p_N^{k+1} = p_0, \end{cases} \tag{22}$$

where

- B_{up} is the $(N + 1) \times (N + 1)^2$ matrix whose entries are equal to 1 at (i, i) with $i \in b_{up}$ and 0 elsewhere;
- B_{down} is the $(N + 1) \times (N + 1)^2$ matrix whose entries are equal to 1 at (i, i) with $i \in b_{down}$ and 0 elsewhere;
- B_{in} is the $(N - 1) \times (N + 1)^2$ matrix whose entries are equal to 1 at (i, i) with $i \in b_{in}$ and 0 elsewhere;
- B_{lat} is the $2(N - 1) \times (N + 1)^2$ matrix whose entries are equal to 1 at (i, i) with $i \in b_{in} \cup b_{out}$ and 0 elsewhere.

Juxtaposing systems (19),(21) and (19),(22), in both cases we end up with a nonlinear system of $6(N + 1)^2 + 8N$ equations in $6(N + 1)^2$ unknowns, which is solved via Newton–Raphson algorithm. The choice of a spectral method was driven by the fact that this type of numerical approach guarantees high accuracy in the solution. Additionally, the computational cost is minimal, as the method involves solving a well-posed nonlinear system of algebraic equations using the Newton–Raphson method at each time step (requiring approximately 30 s of total computational time). The iterative nature of the Newton–Raphson algorithm helps reduce overall computational time, with convergence typically achieved after just 4 to 6 iterations per time step. It is important to emphasize that this is not a numerical paper, and therefore, our goal is not to identify the "optimal" or "practical" numerical scheme. Rather, our primary objective is to obtain a numerical solution that can be compared with those presented in [9].

5. Simulations and results

5.1. Non-monotone cases

We make a comparison between the results obtained through the numerical method described in Section 4 and those of the linear stability analysis carried out by Calusi et al. [9]. Moreover, we are

[2] Here the indices are considered with respect to the lexicographic order.
[3] If $A = (a_{ij}) \in \mathbb{R}^{m\times n}$ and $C = (c_{ij}) \in \mathbb{R}^{p\times q}$, then $A \otimes_K C = (a_{ij}C) \in \mathbb{R}^{mp\times nq}$.

Table 1
Values of the solutions $u_{y,1}$, $u_{y,2}$, $u_{y,3}$ and of their corresponding basins of attraction for $n = -0.9, -0.8, -0.7, -0.5, -0.4$, $\tau_0 = 1.15$, $\alpha = 0.8$, $\beta = 0.01$, Re = 1. The first three values of n correspond to a non-monotone model, while the last two give rise to a monotone law.

n	$u_{y,1}$	$u_{y,2}$	$u_{y,3}$	Basin of attraction of $u_{y,1}$	Basin of attraction of $u_{y,2}$	Basin of attraction of $u_{y,3}$
−0.9	1.72339	3.88349	104.697	(0, 1.9)	–	(103.5, 105.7)
−0.8	1.558	6.38483	90.7802	(0, 2.1)	–	(89.3, 91.8)
−0.7	1.45414	17.1281	51.1502	(0, 2.4)	–	(50, 52.5)
−0.5	1.32013	–	–	(0, 3.8)	–	–
−0.4	1.2723	–	–	(0, 4.7)	–	–

interested in investigating the behaviour over time of our solutions in order to find out, starting from suitable initial conditions, whether they tend to the corresponding stationary one or not. First we focus on the case of prescribed shear stress. With regard to the values of the involved parameters, we take $n = -0.7$, $\beta = 0.01$, $\alpha = 0.8$, Re $= 1$, $\tau_0 = 1.15$, wherein n, β and τ_0 fulfil conditions (3) and (14). We note that even if we change the value of n, the stability results remain unchanged. Indeed, in Table 1 we display the values of the solutions $u_{y,1}$, $u_{y,2}$, $u_{y,3}$ and their corresponding basins of attraction for $n = -0.9, -0.8, -0.7, -0.5, -0.4$ (while the other parameters are fixed), including both the case of non-monotone and monotone model.

First we assume a stress-free configuration as initial condition for system (19), namely we suppose that the flow is not subject to any deformation at time $t = 0$ (i.e. $u_y(t = 0) = 0$). In Fig. 6 we display the resulting plots of the longitudinal velocity $u(y, t)$ as a function of y for different time values and for $x = 0.5$. It is evident that the problem can be seen as a one-dimensional problem since the evolution of the transversal velocity v is almost nonexistent and, consequently, by using the constraint of incompressibility, u can be considered a function of the sole y as spatial variable and of time t. The non-dependence on x is evident from the plots corresponding to other values of x, where the resulting figures are identical. In Fig. 6, we can notice that, for short times, the velocity varies non-linearly with y, while, considering further times, u becomes a linear function of y, as it tends to the steady solution of the form $u_{steady} = u_{y,1}\, y$, where $u_{y,1} = 1.45414$ is the first solution determined in Section 3.1. Then, we assume to have a deformation at time $t = 0$ placed on the right hand side of $u_{y,1}$ on the flow curve before the local maximum $(u_{y,M}, f_M)$, i.e. $u_y(t = 0) = 2.3$. The plots of the corresponding solution are shown in Fig. 7, from which we can see that the longitudinal velocity tends to the basic solution in this case, but u has essentially the same behaviour as before. More precisely, we find that if the initial perturbation is such that $u_y(t = 0)$ is in $(0, 2.4)$, then it converges to the steady flow, while outside of this range the code does not converge. Therefore, we can infer that, starting from a configuration $(\tau, \dot{\gamma})$ belonging to the first ascending branch of the constitutive law with $\dot{\gamma}$ in the range $(0, 1.2)$ (using (10)), the longitudinal velocity tends to the stationary solution of the corresponding branch, and so this confirms the fact that it is unconditionally linearly stable. Now, we study the behaviour in the vicinity of the third basic solution. To this aim, we suppose to start from an initial state with $u_y(t = 0) = 50$ close to the steady solution $u_{y,3} = 51.1502$ on the second ascending branch. To avoid convergence issues, the initial configuration has to be such that $u_y(t = 0)$ is in the range $(50, 52.5)$. In Fig. 8 we display the plots of the corresponding velocity for time $t = 1, 15$ (for admissible initial deformations on the right side of $u_{y,3}$ there is no difference in the plots). From Fig. 8 we can infer that the third solution found in Section 3.1 is stable too, but only in the case of small perturbations, more precisely for $\dot{\gamma}$ in $(25, 26.25)$. Thus, the result of linear stability determined in [9] is confirmed, since our numerical solution tends to the steady one, but its basin of attraction is very small. Finally, regarding the solution $u_{y,2} = 17.1281$ belonging to the descending branch, assuming any point between the local maximum and minimum as initial condition, we are not able to obtain the corresponding stationary solution even if we start from a perturbation with $u_y(t = 0) = 17.128$. This is due to the fact that $u_{y,2}$ is (linearly) unconditionally unstable.

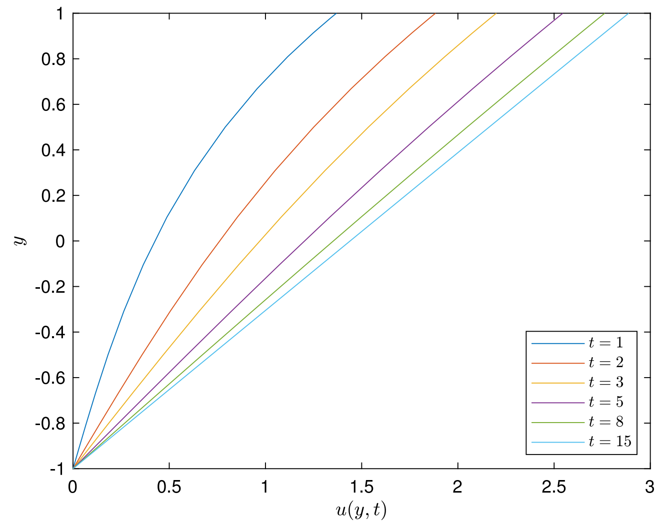

Fig. 6. Plot of $u(y, t)$ for $t = 1, 2, 3, 5, 8, 15$, $x = 0.5$, $n = -0.7$, $\beta = 0.01$, $\alpha = 0.8$, Re $= 1$, $\tau_0 = 1.15$ with $u_y(t = 0) = 0$.

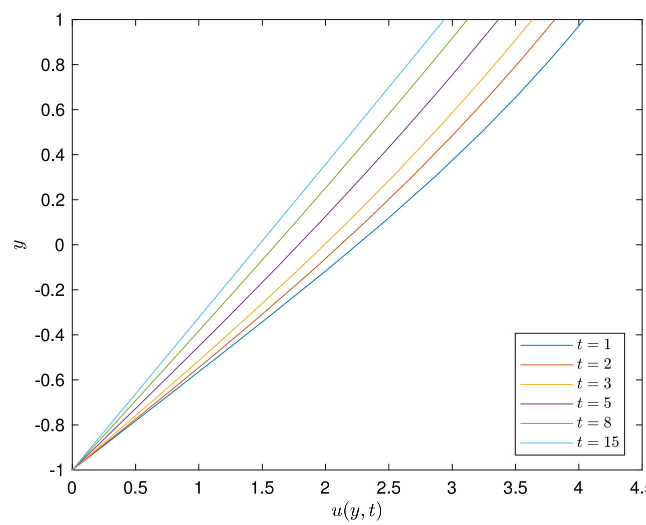

Fig. 7. Plot of $u(y, t)$ for $t = 1, 2, 3, 5, 8, 15$, $x = 0.5$, $n = -0.7$, $\beta = 0.01$, $\alpha = 0.8$, Re $= 1$, $\tau_0 = 1.15$ with $u_y(t = 0) = 2.3$.

Regarding the case of the other boundary conditions, we perform the same analysis for the three different solutions $u_{y,1} = 1.74991$, $u_{y,2} = 10.5968$, $u_{y,3} = 70.9461$ found in Section 3.2. For the involved parameters, we take $n = -0.7$, $\beta = 0.01$, $\alpha = 0.8$, Re $= 1$, $u_0 = 3.5$, wherein n, β and u_0 fulfil conditions (3) and (17). In Figs. 9, 10, 11, we display the plots of u starting from an initial perturbation with $u_y(t = 0) = 0$, $u_y(t = 0) = 2.5$ and $u_y(t = 0) = 69.5$ respectively.

The basins of attraction of $u_{y,1} = 1.74991$ and $u_{y,3} = 70.9461$ are $(0, 2.5)$ and $(69.5, 72.5)$ (expressed in terms of $u_y(t = 0)$, or equivalently in terms of $\dot{\gamma}$ $(0, 1.25)$ and $(34.75, 36.25)$) respectively. On the other hand, if

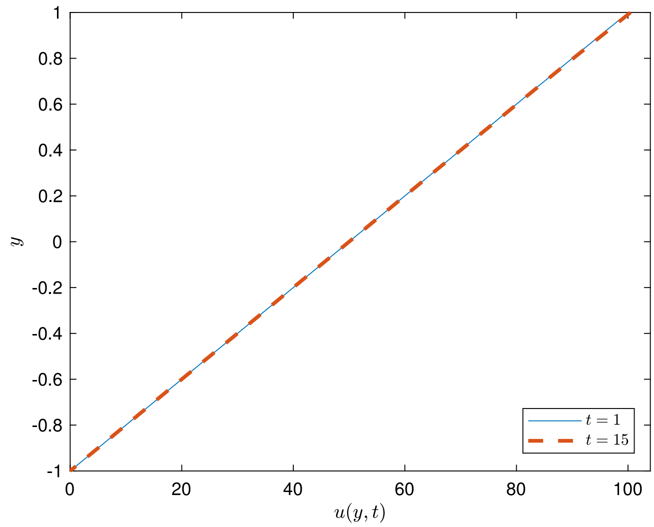

Fig. 8. Plot of $u(y,t)$ for $t = 1, 15$, $x = 0.5$, $n = -0.7$, $\beta = 0.01$, $\alpha = 0.8$, $\mathrm{Re} = 1$, $\tau_0 = 1.15$ with $u_y(t = 0) = 50$.

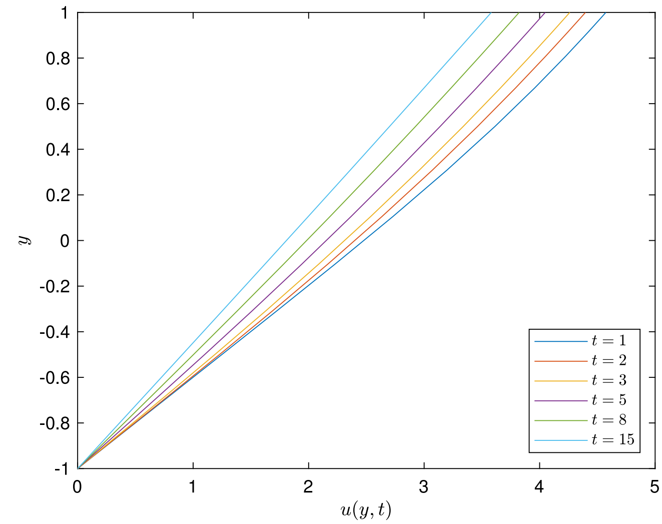

Fig. 10. Plot of $u(y,t)$ for $t = 1, 2, 3, 5, 8, 15$, $x = 0.5$, $n = -0.7$, $\beta = 0.01$, $\alpha = 0.8$, $\mathrm{Re} = 1$, $u_0 = 3.5$ with $u_y(t = 0) = 2.5$.

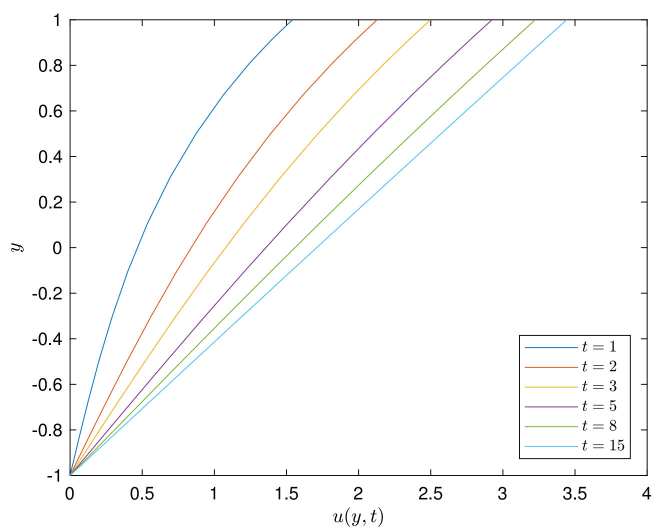

Fig. 9. Plot of $u(y,t)$ for $t = 1, 2, 3, 5, 8, 15$, $x = 0.5$, $n = -0.7$, $\beta = 0.01$, $\alpha = 0.8$, $\mathrm{Re} = 1$, $u_0 = 3.5$ with $u_y(t = 0) = 0$.

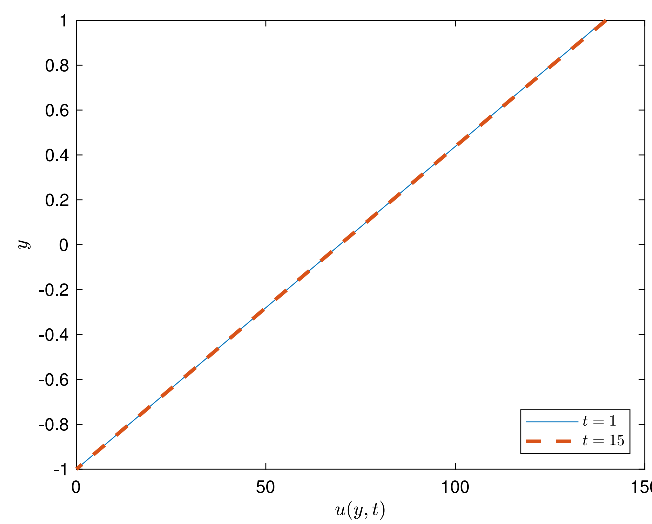

Fig. 11. Plot of $u(y,t)$ for $t = 1, 15$, $x = 0.5$, $n = -0.7$, $\beta = 0.01$, $\alpha = 0.8$, $\mathrm{Re} = 1$, $u_0 = 3.5$ with $u_y(t = 0) = 69.5$.

we consider $u_{y,2} = 10.5968$, the code does not converge even if we start from the solution itself. Therefore, we can draw the same conclusions as before, since there is no difference with respect to the behaviours found under the hypothesis of Neumann boundary conditions.

5.2. Monotone case

Now we repeat the simulations assuming a monotone relation between stress and strain rate under the hypothesis of prescribed shear stress imposed on the top surface. With regard to the values of the involved parameters, we take $n = -0.5$, $\beta = 0.1$, $\alpha = 0.8$, $\mathrm{Re} = 1$, $\tau_0 = 3$. The single solution to investigate is $u_{y,1} = 8.39301$ found in Section 3.3. In Figs. 12 and 13 we display the plots of u starting from a stress free configuration (i.e. $u_y(t = 0) = 0$) and from a point placed on the right side of $u_{y,1}$ (i.e. $u_y(t = 0) = 15$) respectively. As we expected, the behaviour is very similar to the one of the solution on the first ascending branch in Section 5.1. In particular we can notice that our numerical solutions tend to the stationary one after sufficiently long time. Thanks to the monotonicity of the model, the basin of attraction of $u_{y,1}$, which is (0,15) expressed in terms of $u_y(t = 0)$, is greater than the one of the non-monotone law. Thus, we confirm that the state solution $u_{y,1}$ is linear unconditionally stable in the monotone case too (as proved in [9]).

6. Conclusions

We have investigated an unsteady Couette flow driven by a prescribed shear stress or a prescribed longitudinal velocity imposed on the top surface, considering a class of fluids described by a non-monotone constitutive equation. Selecting proper values for the involved parameters, the corresponding stress vs strain-rate relation is a non-monotone function. The main motivation of this study is to confirm numerically the findings of [9], in which the authors proved that, in the case of multiple basic solutions, the stable ones are those corresponding to the ascending branches of the flow curve.

In the 1D steady case, both under the hypothesis of Neumann and Dirichlet boundary conditions, we have recovered three basic steady-state solutions as provided by Calusi et al. [9]. Regarding the 2D unsteady case, both problems have been reduced to an initial and

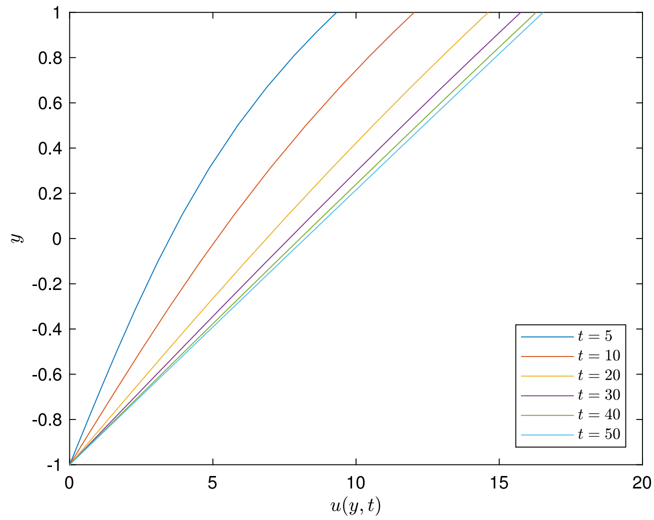

Fig. 12. Plot of $u(y,t)$ for $t = 5, 10, 20, 30, 40, 50$, $x = 0.5$, $n = -0.5$, $\beta = 0.1$, $\alpha = 0.8$, $\mathrm{Re} = 1$, $\tau_0 = 3$ with $u_y(t = 0) = 0$.

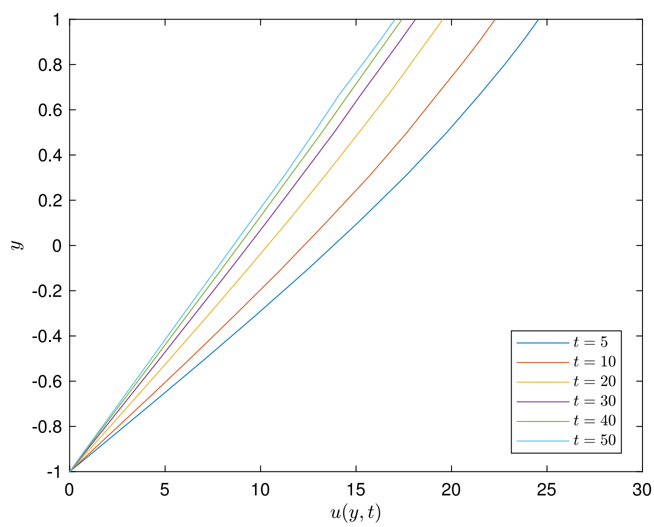

Fig. 13. Plot of $u(y,t)$ for $t = 5, 10, 20, 30, 40, 50$, $x = 0.5$, $n = -0.5$, $\beta = 0.1$, $\alpha = 0.8$, $\mathrm{Re} = 1$, $\tau_0 = 3$ with $u_y(t = 0) = 15$.

boundary value problem that we have solved by means of Crank–Nicolson method combined with spectral collocation method. Starting from various initial conditions in each of the two cases, we have studied the behaviour of the numerical solutions and we have confirmed numerically the linear stability analysis performed in [9]. In particular, regardless of the type of boundary conditions, the two basic solutions belonging to the ascending branches of the constitutive law are unconditionally linearly stable, while the one on the descending branch is linearly unstable. Moreover, the basin of attraction of the second stable solution is much smaller than the one of the first. The final result is consistent with the analysis presented in [9]. Specifically, the stability analysis in [9] is linear, implying that the perturbations are small. Consequently, to verify the convergence of the numerical solution, we must start from an initial configuration that is sufficiently close to the stationary solution. In this work, we have shown that if the initial state lies on the first ascending branch – though not necessarily close to the stationary solution – the numerical solution still converges to the stationary state. This suggests that the solution is "more" than linearly stable on the first ascending branch. However, this is not true for the second ascending branch, where the initial state must be very close to the stationary solution for convergence to occur. Finally, in the descending branch, even when starting exactly at the stationary solution, the numerical solution diverges, indicating that the system is unconditionally unstable. We have considered also the case of a monotone constitutive law, selecting different values for the involved parameters. We have found the existence of a single steady solution. It has the same behaviour of the state solution on the first ascending branch in the non-monotone model, meaning that it is linear unconditionally stable and maybe "more" than linearly thanks to the amplitude of its basin of attraction. In conclusion, this work seems to indicate that in the non-monotone case (1) the first ascending branch is nonlinearly stable, (2) the descending branch is unconditionally unstable, (3) the second ascending branch is only linearly stable. Of course, point (1) and the possible "more than linear" stability of the single solution in the monotone case are just guesses that must be confirmed by a rigorous nonlinear stability analysis.

CRediT authorship contribution statement

Lorenzo Fusi: Writing – review & editing, Writing – original draft. **Antonio Giovinetto:** Writing – review & editing, Writing – original draft. **Rebecca Tozzi:** Writing – review & editing, Writing – original draft.

Declaration of competing interest

The authors declare that they have no known competing financial interests or personal relationships that could have appeared to influence the work reported in this paper.

Acknowledgements

The present work has been performed under the auspices of the Italian National Group for Mathematical Physics (GNFM-Indam). This work has been done under the framework PRIN 2022 project "Mathematical modelling of heterogeneous systems" financed by the European Union - Next Generation EU, CUP B53D23009360006/B53D23009370006, Project Code 2022MKB7MM, PNRR M4.C2.1.1.

Data availability

No data was used for the research described in the article.

References

[1] K.R. Rajagopal, On implicit constitutive theories for fluids, J. Fluid Mech. 550 (2006) 243–249.
[2] L. Fusi, A. Farina, Flow of a class of fluids defined via implicit constitutive equation down an inclined plane: Analysis of the quasi-steady regime, Eur. J. Mech. B Fluids 61 (2017) 200–208.
[3] L. Fusi, A. Ballotti, Squeeze flow of stress power law fluids, Fluids 6 (6) (2021) 194.
[4] L. Fusi, G. Saccomandi, K.R. Rajagopal, L. Vergori, Flow past a porous plate of non-Newtonian fluids with implicit shear stress shear rate relationships, Eur. J. Mech. B Fluids 92 (2022) 166–173.
[5] R. Bustamante, K.R. Rajagopal, O. Orellana, R. Meneses, Implicit constitutive relations for describing the response of visco-elastic bodies, Int. J. Non-Linear Mech. 126 (2020) 103526.
[6] K.R. Rajagopal, On implicit constitutive theories, Appl. Math. 48 (2003) 279–319.
[7] K.R. Rajagopal, A review of implicit algebraic constitutive relations for describing the response of nonlinear fluids, C. R. Méc. 351 (S1) (2023) 703–720.
[8] K.R. Rajagopal, The mechanics and mathematics of bodies described by implicit constitutive equations, in: Mathematical Analysis of Continuum Mechanics and Industrial Applications III: Proceedings of the International Conference CoMFoS18 18, Springer, 2020, pp. 49–65.
[9] B. Calusi, L. Fusi, A. Farina, Linear stability of a couette flow for non-monotone stress-power law models, Eur. Phys. J. Plus 138 (10) (2023) 933.
[10] L. Fusi, B. Calusi, A. Farina, K.R. Rajagopal, On the flow of a stress power-law fluid in an orthogonal rheometer, Int. J. Non-Linear Mech. 149 (2023) 104306.

[11] T. Perlacova, V. Prusa, Tensorial implicit constitutive relations in mechanics of incompressible non-Newtonian fluids, J. Non-Newton. Fluid Mech. 216 (2015) 13–21.
[12] V. Prusa, K.R. Rajagopal, On implicit constitutive relations for materials with fading memory, J. Non-Newton. Fluid Mech. 181 (2012) 22–29.
[13] K.R. Rajagopal, A.R. Srinivasa, On the thermodynamics of fluids defined by implicit constitutive relations, Z. Angew. Math. Phys. 59 (2008) 715–729.
[14] J. Malek, V. Prusa, K.R. Rajagopal, Generalizations of the Navier–Stokes fluid from a new perspective, Internat. J. Engrg. Sci. 48 (12) (2010) 1907–1924.
[15] C. Le Roux, K.R. Rajagopal, Shear flows of a new class of power-law fluids, Appl. Math. 58 (2) (2013) 153–177.
[16] V. Zarnitsina, A. Pokhilko, F. Ataullakhanov, A mathematical model for the spatio-temporal dynamics of intrinsic pathway of blood coagulation. I. The model description, Thromb. Res. 84 (4) (1996) 225–236.
[17] V. Zarnitsina, A. Pokhilko, F. Ataullakhanov, A mathematical model for the spatio-temporal dynamics of intrinsic pathway of blood coagulation. II. Results, Thromb. Res. 84 (5) (1996) 333–344.
[18] M. Anand, K.R. Rajagopal, A model incorporating some of the mechanical and biochemical factors underlying clot formation and dissolution in flowing blood, Comput. Math. Methods Med. 5 (3–4) (2003) 183–218.
[19] M. Anand, K.R. Rajagopal, A model for the formation and lysis of blood clots, Pathophysiol. Haemost. Thromb. 34 (2–3) (2006) 109–120.
[20] J. Crank, P. Nicolson, A practical method for numerical evaluation of solutions of partial differential equations of the heat-conduction type, in: Mathematical Proceedings of the Cambridge Philosophical Society, Vol. 43, Cambridge University Press, 1947, pp. 50–67.
[21] L. Fusi, A. Giovinetto, A spectral collocation scheme for the two dimensional flow of a regularized viscoplastic fluid: Numerical results and comparison with analytical solution, Math. Comput. Simulation (2024).
[22] L. Fusi, A. Giovinetto, A spectral collocation scheme for the flow of a piezo-viscous fluid in ducts with slip conditions, Theor. Comput. Fluid Dyn. (2024) 1–22.
[23] L.N. Trefethen, Spectral Methods in MATLAB, SIAM, 2000.